PLOS ONE

RESEARCH ARTICLE

TNF-α inhibitor reduces drug-resistance to anti-PD-1: A mathematical model

Xiulan Lai[1], **Wenrui Hao**[2], **Avner Friedman**[3]*

1 Institute for Mathematical Sciences, Renmin University of China, Beijing, P. R. China, **2** Department of Mathematics, Pennsylvania State University, State College, PA, United States of America, **3** Mathematical Bioscience Institute & Department of Mathematics, Ohio State University, Columbus, OH, United States of America

* afriedman@math.osu.edu

Citation: Lai X, Hao W, Friedman A (2020) TNF-α inhibitor reduces drug-resistance to anti-PD-1: A mathematical model. PLoS ONE 15(4): e0231499. https://doi.org/10.1371/journal.pone.0231499

Editor: Dominik Wodarz, University of California Irvine, UNITED STATES

Received: November 11, 2019

Accepted: March 24, 2020

Published: April 20, 2020

Data Availability Statement: All relevant data are within the paper.

Funding: XL was partially supported by the Fundamental Research Funds for the Central Universities (19XNLG14), and the Research Funds of Renmin University of China, and National Natural Science Foundation of China (11571364). WH was partially supported by the National Science Foundation (Grant DMS-1818769).

Competing interests: The authors have declared that no competing interests exist.

Abstract

Drug resistance is a primary obstacle in cancer treatment. In many patients who at first respond well to treatment, relapse occurs later on. Various mechanisms have been explored to explain drug resistance in specific cancers and for specific drugs. In this paper, we consider resistance to anti-PD-1, a drug that enhances the activity of anti-cancer T cells. Based on results in experimental melanoma, it is shown, by a mathematical model, that resistances to anti-PD-1 can be significantly reduced by combining it with anti-TNF-α. The model is used to simulate the efficacy of the combined therapy with different range of doses, different initial tumor volume, and different schedules. In particular, it is shown that under a course of treatment with 3-week cycles where each drug is injected in the first day of either week 1 or week 2, injecting anti-TNF-α one week after anti-PD-1 is the most effective schedule in reducing tumor volume.

Introduction

Drug resistance is one of the primary causes for suboptimal outcomes in cancer therapy [1]. Patients respond well at first, but relapse occurs for many cancer patients [2]. One common resistance is associated with the ATP-binding cassette (ABC) transporters. These protein pumps act to protect cells by ejecting variety of toxins, and they are overexpressed during anti-cancer treatment with chemotherapy and targeted therapy [1–3].

Other mechanisms of drug resistance are associated with mutations and epigenetic changes [4]. There are many mathematical models of drug resistance, particularly resistance to chemotherapy; e.g., a model of evolution of resistance [5], and a model of resistance associated with symmetric/asymmetric division of stem cells [6]. Article [7] reviews the mathematical models up to 2011, and very recent reviews are found in [8, 9]. Recent models considered multi-mutations in drug resistance for specific cases [10], and optimal therapy design to reduce drug resistance [11]. A list of the mathematical and computational methods used to simulate models of drug resistance are given in [12, 13]; in particular, articles [4, 14] use PDE models, as do the recent papers [15, 16] and the present one.

There are different mechanisms of resistance to different drugs. In this paper we consider resistance to the immunotherapy drug anti-PD-1, and show that injection of TNF-α will reduce the resistance.

PD-1 is a checkpoint on T cells. Its ligand PD-L1 is expressed on both T cells and cancer cells. The formation of the complex PD-1-PD-L1 initiates a signaling cascade that results in blocking the anti-cancer activity of T cells. PD-1 blockade by anti-PD-1 drugs, is currently increasing used in the treatment of cancers.

Internal mechanisms of drug resistance to anti-PD-1 include the following:

- **B2M mutation:** Loss of b2-microglobulin (B2M) expression results in impaired cell surface expression of HLA class I (MHC class I), which in turn impairs antigen presentation to cytotoxic T cells, and thereby leads to anti-PD-1 resistance [17–20].
- **JAK-1/JAK-2 mutation:** INF-γ released by T cells activates the signalling pathway. JAK1/JAK2-STAT1/STAT2/STAT3-IRF1, which leads to upregulation of PD-L1 on cancer cells [21]. Acquired resistance to PD-1 blockade immunotherapy in patients with melanoma was associated with defects in the pathways involved in interferon-receptor signaling, such as mutation of interferon-receptor-associated Janus kinase 1 (JAK1) or Janus kinase 2 (JAK2) [17, 20, 22]. Inability to respond to IFN-γ leads to reduced expression of PD-L1 on cancer and hence to reduced effectiveness of anti-PD-1.
- **Loss of neoantigen:** Genetic mutations that make cells become cancer cells may result in production of proteins that immune system can recognize as antigen; these are called neoantigens. Anti-PD-1 treatment may cause mutations in cancer cells that result in loss of neoantigens, and, correspondingly, to a decrease in immune response, including decreases in the number of active anti-cancer T cells, and hence a decrease in the effectiveness of anti-PD-1 [23].

Another form of drug resistance is associated with a change undergoing in the anti-cancer $CD8^+$ T cells (cytotoxic T cells, CTLs):

- **TIM-3 checkpoint:** Under anti-PD-1 treatment, T-cell immunoglobulin mucin-3 (TIM-3) is upregulated on T cells [24]. Its ligand, Galectin-9 (Gal-9) is expressed on cancer cells, and the complex formed by the checkpoint TIM-3 and its ligand Gal-9 induces apoptosis of Th1 cells [25, 26], and, consequently, a reduction in $CD8^+$ T cells whose proliferation depends on Th1-secreted IL-2.

Recent approaches to overcome anti-PD-1 drug resistance focus on combination strategies [27]. A prime example is the combination of anti-PD-1 and anti-CTL-4 [28–31].

TNF-α is a pleiotropic cytokine that is involved in diverse functions. In immune response to cancer it acts as immunosuppressive [32]. TNF-α has been shown to enhance the expression of PD-L1 on $CD8^+$ T cells in cancer [33], including melanoma [34]. TNF-α elicits an increase in TIM-3+ $CD8^+$ T cells, and anti-PD-1 triggers TIM-3 expression in TNF-α dependent manner [32]. Hence blockade of TNF-α overcomes resistance to anti-PD-1 by reducing TIM-3 and PD-L1 expression.

For simplicity, we shall combine $CD4^+$ Th1 cells with $CD8^+$ T cells, since they play similar roles in the response to anti-PD-1 drug resistance, and refer to the combined populaltion of T cells as cytotoxic lymphocytes (CTL).

In the present paper we develop a mathematical model of combination therapy with anti-PD-1 and anti-TNF-α. The model will be used to simulate the efficacy of anti-PD-1 under different amount of anti-TNF-α, and under different schedules of treatment.

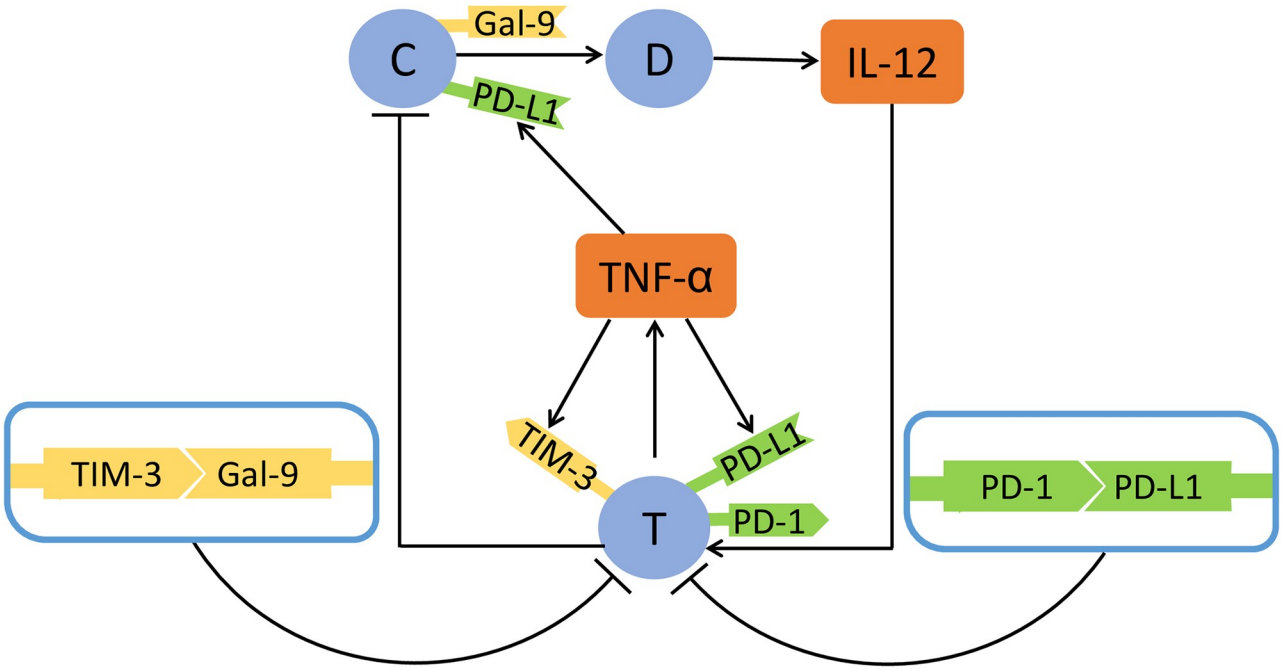

Fig 1. Interaction of immune cells with cancer cells. Sharp arrows indicate proliferation/activation, blocked arrows indicate killing/blocking. C: cancer cells, D: dendritic cells, *T*: activated CTL cells. T cells express PD-1, PD-L1, TIM-3; cancer cells express PD-L1 and Gal-9.

https://doi.org/10.1371/journal.pone.0231499.g001

The model includes the densities of cancer cells (C), dendritic cells (D) and CTL cells (T), the concentrations of cytokines TNF-α and IL-12, and the proteins PD-1, PD-L1, TIM-3 and Gal-9. Resistance to anti-PD-1 treatment is modeled by upregulation of TIM-3 [24]. The model is based on the network shown in Fig 1, and will be represented by a system of partial differential equations.

The model equations

The list of variables is given in Table 1 in unit of g/cm^3; the unit of time is taken to be 1 day. We assume that the total density of cells within three tumor remains constant in space and

Table 1. List of variables (in units of g/cm^3).

Notation	Description
C	density of cancer cells
D	density of dendritic cells
T	density of activated CTL cells
T_α	TNF-α concentration
I_{12}	IL-12 concentration
P	PD-1 concentration
L	PD-L1 concentration
Q_1	PD-1-PD-L1 concentration
Q_2	TIM-3-Gal-9 concentration
T_M	TIM-3 concentration
G	Gal-9 concentration
A	anti-PD-1 (e.g. nivolumab)
B	anti-TNF-α (e.g. infliximab)

https://doi.org/10.1371/journal.pone.0231499.t001

time:

$$D + T + C = \text{constant}. \tag{1}$$

Under the assumption (1), proliferation of cancer cells and immigration of immune cells into the tumor give rise to internal pressure among the cells, which results in cells movement. We assume that all the cells move with the same velocity, **u**; **u** depends on space and time and will be taken in units of cm/day. We also assume that all the cells undergo dispersion (i.e., diffusion), and that all the cytokines and anti-tumor drugs are also diffusing within the tumor.

Equations for DCs (D)

By necrotic cancer cells we mean cancer cells undergoing the process of necrosis. Necrotic cancer cells release HMGB-1 [35]. Dendritic cells are activated by HMGB-1 [36, 37], and we assume that the density of HMGB-1 is proportional to the density of cancer cells. Hence the dynamics of activated dendritic cells is given by

$$\frac{\partial D}{\partial t} + \underbrace{\nabla \cdot (\mathbf{u}D)}_{\text{velocity}} - \underbrace{\delta_D \nabla^2 D}_{\text{difusion}} = \underbrace{\lambda_{DC}\hat{D}_0 \frac{C}{K_C + C}}_{\text{activation by necrotic cells}} - \underbrace{d_D D}_{\text{death}}, \tag{2}$$

where $\hat{D}_0$ is the density of immature dendritic cells which we assume to be constant, δ_D is the dispersion (or diffusion) coefficients of DCs, and d_D is the death rate of DCs.

Equations for CTL cells (T)

Inactive T cells are activated by IL-12 [38, 39]. The processes of activation and proliferation of T cells are inhibited by the complexes PD-1-PD-L1 (Q_1) and TIM-3-Gal-9 (Q_2). We represents these inhibitions by factors $\frac{1}{1+Q_1/K'_{TQ_1}}$ and $\frac{1}{1+Q_2/K'_{TQ_2}}$, respectively, and take (see Eq (10)) $\frac{1}{1+Q_1/K'_{TQ_1}} = \frac{1}{1+PL/K_{TQ_1}}$ and, similarly, $\frac{1}{1+Q_2/K'_{TQ_2}} = \frac{1}{1+T_M G/K_{TQ_2}}$. Hence T satisfies the following equation:

$$\begin{aligned} \frac{\partial T}{\partial t} + \nabla \cdot (\mathbf{u}T) - \delta_T \nabla^2 T \quad = \quad & \underbrace{\lambda_{TI_{12}} \hat{T}_0 \cdot \frac{I_{12}}{K_{I_{12}} + I_{12}}}_{\text{activation by IL-12}} \cdot \underbrace{\frac{1}{1 + PL/K_{TQ_1}}}_{\text{inhibition by PD-1-PD-L1}} \\ & \times \underbrace{\frac{1}{1 + T_M G/K_{TQ_2}}}_{\text{inhibition by TIM-3-Gal-9}} - \underbrace{d_T T}_{\text{death}} \end{aligned} \tag{3}$$

where $\hat{T}_0$ is the density of the inactive T cells.

Equation for tumor cells (C)

We assume a logistic growth for cancer cells with carrying capacity (C_M) in order to account for competition for space among these cells. Cancer cells are killed by T cells. The equation for C takes the form:

$$\frac{\partial C}{\partial t} + \nabla \cdot (\mathbf{u}C) - \delta_C \nabla^2 C = \underbrace{\lambda_C C\left(1 - \frac{C}{C_M}\right)}_{\text{proliferation}} - \underbrace{\eta T C}_{\text{killing byTcells}} - \underbrace{d_C C,}_{\text{death}} \tag{4}$$

where η are the killing rates of cancer cells by T, and d_C is the natural death rate of cancer cells (by apoptosis).

Equation for IL-12 (I_{12})

The proinflammatory cytokine IL-12 is secreted by activated DCs [38, 39], so that

$$\frac{\partial I_{12}}{\partial t} - \delta_{I_{12}} \nabla^2 I_{12} = \underbrace{\lambda_{I_{12}D} D}_{\text{production by DCs}} - \underbrace{d_{I_{12}} I_{12}}_{\text{degradation}}. \tag{5}$$

Since the diffusion coefficients of proteins are very large compared to those of cells, their advection velocity may be neglected.

Equation for TNF-α (T_α)

Macrophages are attracted to the tumor, and they produce TNF-α [40]. For simplicity, we do not include macrophages in the model, and represent their TNF-α contribution as a source A_{T_α}. The cytokine TNF-α is also secreted by T cells, so that

$$\frac{\partial T_\alpha}{\partial t} - \delta_{T_\alpha} \nabla^2 T_\alpha = A_{T_\alpha} + \underbrace{\lambda_{T_\alpha T} T}_{\text{production byTcells}} - \mu_{T_\alpha B} T_\alpha B - \underbrace{d_{T_\alpha} T_\alpha}_{\text{degradation}}, \tag{6}$$

where B is the TNF-α inhibitor.

Equation for PD-1 (P), PD-L1 (L) and PD-1-PD-L1 (Q_1)

PD-1 is expressed on the surface of activated $CD8^+$ T cells [41, 42]. We denote by ρ_T the mass of all the PD-1 in one T cell divided by the mass of a T cell, so that

$$P = \rho_P T. \tag{7}$$

PD-L1 is expressed on the surface of activated $CD8^+$ T cells [42] and cancer cells [42, 43]. We denote by ρ_L the mass of all the PD-L1 in one T cell divided by the mass of the cell, and by $\rho_L \varepsilon_C$ the mass of all the PD-L1 in one cancer cell divided by the mass of the cell, so that

$$L = \rho_L (T + \varepsilon_C C).$$

The expression of PD-L1 is upregulated by TNF-α [33], so that

$$L = \rho_L (T + \varepsilon_C C) \left(1 + \alpha_L \frac{T_\alpha}{K_{T_\alpha} + T_\alpha}\right). \tag{8}$$

The coefficient ρ_P is constant when no anti-PD-1 drug is administered. And in this case, to a change in T, given by $\frac{\partial T}{\partial t}$, there corresponds a change of P, given by $\rho_P \frac{\partial T}{\partial t}$. For the same reason, $\nabla \cdot (\mathbf{u}P) = \rho_P \nabla \cdot (\mathbf{u}P)$ and $\nabla^2 P = \rho_P \nabla^2 P$ when no anti-PD-1 drug is injected. Hence, P satisfies the equation

$$\frac{\partial P}{\partial t} + \nabla \cdot (\mathbf{u}P) - \delta_T \nabla^2 P = \rho_P \left[\frac{\partial T}{\partial t} + \nabla \cdot (\mathbf{u}T) - \delta_T \nabla^2 T\right].$$

Recalling Eq (3) for T, we get

$$\frac{\partial P}{\partial t} + \nabla \cdot (\mathbf{u}P) - \delta_T \nabla^2 P = \quad \rho_P[\text{RHS of Eq. (3)}].$$

When anti-PD-1 drug (A) is applied, PD-1 is depleted by A, and the ratio $\frac{P}{T}$ may change. In order to include in the model both cases of with and without anti-PD-1, we replace ρ_P in the previous equation by $\frac{P}{T}$. Hence,

$$\frac{\partial P}{\partial t} + \nabla \cdot (\mathbf{u}P) - \delta_T \nabla^2 P = \quad \frac{P}{T}[\text{RHS of Eq. (3)}] - \underbrace{\mu_{PA} PA}_{\text{depletion by anti-PD-1}}, \tag{9}$$

where μ_{PA} is the depletion rate of PD-1 by anti-PD-1.

PD-L1 from T cells or cancer cells combines with PD-1 on the plasma membrane of T cells to form a complex PD-1-PD-L1 (Q_1) on the T cells [42, 43]. Denoting the association and dis-association rates of Q_1 by α_{PL} and d_{Q_1}, respectively, we can write

$$P + L \underset{d_{Q_1}}{\overset{\alpha_{PL}}{\rightleftharpoons}} Q_1.$$

The half-life of Q_1 is less then 1 second (i.e. 1.16×10^{-5} day) [44], so that d_{Q_1} is very large. Hence we may approximate the dynamical equation for Q_1 by the steady state equation, $\alpha_{PL} PL = d_{Q_1} Q_1$, or

$$Q_1 = \sigma_1 PL, \tag{10}$$

where $\sigma_1 = \alpha_{PL}/d_{Q_1}$. Hence, $K'_{TQ_1} = \sigma_1 K_{TQ_1}$.

Equation for TIM-3 (T_M), Gal-9 (G) and TIM-3-Gal-9 (Q_2)

TIM-3 is expressed on the surface of activated $CD8^+$ T cells. If we denote by ρ_M the ratio between the mass of all the TIM-3 proteins in one T cell and the mass of one T cell, then

$$T_M = \rho_M T.$$

The expression of TIM-3 is enhanced by TNF-α [32], and further upregulated by anti-PD-1 [24, 32], so that

$$T_M = \rho_M T \left[1 + \alpha_T \frac{T_\alpha}{K_\alpha + T_\alpha} \left(1 + \alpha_{MA} \frac{A}{K_A + A}\right)\right]. \tag{11}$$

Gal-9 is expressed on the surface of cancer cells. We denote by ρ_G the ratio between the mass of all the Gal-9 proteins in one cancer cell and the mass of a cancer cell, so that

$$G = \rho_G C. \tag{12}$$

Similarly to Eq (10), we represent the concentration of the complex TIM-3-Gal-9 in the form:

$$Q_2 = \sigma_2 T_M G, \tag{13}$$

Hence, $K'_{TQ_2} = \sigma_2 K_{TQ_2}$.

From Eq (11), we see that resistance to anti-PD-1 is due to upregulation of TIM-3 [24], as represented by the parameter α_{MA}, but the level of resistance depends on the concentration of TNF-α. This suggests that anti-TNF-α will reduce resistance to anti-PD-1.

Equation for anti-PD-1 (A)

We shall consider simple mice experiments where the anti-PD-1 drug is administered in equal amount γ_A at days $t_1, t_2, \ldots$, and set $\gamma_A(t) = \gamma_A \sum_{t_i<t} e^{-\beta(t-t_i)}$ for some $\beta > 0$. Some of the drug is depleted in the process of blocking PD-1 and some is degraded, or washed out at rate d_A. Hence A satisfies the following equation:

$$\frac{\partial A}{\partial t} - \delta_A \nabla^2 A = \gamma_A(t) - \underbrace{\mu_{PA} PA}_{\text{depletion through blocking PD}-1} - \underbrace{d_A A.}_{\text{degradation}} \tag{14}$$

Equation for anti-TNF-α (B)

Similarly to Eq (14), we take the dynamics of B to be:

$$\frac{\partial B}{\partial t} - \delta_B \nabla^2 B = \gamma_B(t) - \underbrace{\mu_{T_\alpha B} T_\alpha B}_{\text{depletion through blocking TNF}-\alpha} - \underbrace{d_B B,}_{\text{degradation}} \tag{15}$$

where $\gamma_B(t) = \gamma_B \sum_{t_i'<t} e^{-\beta(t-t_i')}$.

Equation for cells velocity (u)

As estimated in the section on parameter estimation, the average steady state densities of the immune cells D, T_8 and C are taken to be (in units of g/cm^3)

$$D = 4 \times 10^{-4},\ T = 1 \times 10^{-3},\ C = 0.4. \tag{16}$$

To be consistent with Eq (1), we take the constant on the RHS of Eq (1) to be 0.4014. We further assume that all cells have approximately the same diffusion coefficient. Adding Eqs (2)–(4), we get

$$0.4014 \times \nabla \cdot \mathbf{u} = \sum_{j=2}^{4} [\text{right} - \text{hand side of Eq. (j)}]. \tag{17}$$

To simplify the computations, we assume that the tumor is spherical and denote its radius by $r = R(t)$. We also assume that all the densities and concentrations are radially symmetric, that is, they are functions of (r, t), where $0 \leq r \leq R(t)$. In particular, $\mathbf{u} = u(r, t)\,\mathbf{e}r$, where $\mathbf{e}_r$ is the unit radial vector.

Equation for free boundary (R)

We assume that the free boundary $r = R(t)$ moves with the velocity of cells, so that

$$\frac{dR(t)}{dt} = u(R(t), t). \tag{18}$$

Boundary conditions. We assume that inactive CTL cells that migrated from the lymph nodes into the tumor microenvironment have constant density $\hat{T}$ at the tumor boundary, and, upon crossing the boundary, they are activated by IL-12. We then have the following flux

conditions for T cells and P at the tumor boundary:

$$\frac{\partial T}{\partial r} + \sigma_T(I_{12})(T - \hat{T}) = 0, \quad \text{at } r = R(t), \tag{19}$$

$$\frac{\partial P}{\partial r} + \sigma_T(I_{12})(P - \rho_P \hat{T}) = 0, \quad \text{at } r = R(t), \tag{20}$$

where we take $\sigma_T(I_{12}) = \sigma_0 \frac{I_{12}}{K_{I_{12}} + I_{12}}$. We also assume

$$\text{no-flux for} \quad D, I_{12}, T_\alpha, A \text{ and } B \text{ at } r = R(t); \tag{21}$$

the boundary condition for C is determined by Eq (1).

Initial conditions. The initial conditions must be consistent with Eqs (1) and (16), namely,

$$D + T + C = 0.4014\ \text{g/cm}^3, \tag{22}$$

and

$$P = \rho_P T \ \ at\ t = 0. \tag{23}$$

The last condition ensures that in the control case (where $A \equiv 0$), the function $P = \rho_P T$ is the solution of Eq (9) with the boundary condition (20). The specific choice of initial conditions for our simulations is

$$\begin{aligned} &D_0 = 2 \times 10^{-4},\ T_0 = 1 \times 10^{-4}, C_0 = 0.4011,\ I_{12,0} = 1 \times 10^{-10},\ T_{\alpha,0} = 1 \times 10^{-11}, \\ &R(0) = 0.5 \text{ cm or } R(0) = 1 \text{ cm}. \end{aligned} \tag{24}$$

However, other choices give similar simulation results after a few days.

Results

The simulations of the model were performed by Matlab based on the moving mesh method for solving partial differential equations with free boundary [45] (see the section on computational method). Fig 2, in the control case (no drugs), shows the average densities of cells and concentrations of cytokines for the first 30 days, and the growth of tumor volume; We note that the average concentrations of each species, X, tends to steady state X^0. In estimating some production parameters (in section of parameter estimation) we made the assumption that each "half-saturation" parameter K_X is equal to X^0, and X^0 is estimated from clinical/experimental data. By comparing the values of K_X in Table 2 with the values X^0 from Fig 2 we see that this assumption is approximately satisfied. Fig 2 shows that, as tumor progresses, the average densities of the anti-cancer immune cells (D, T) increase, as do the average concentrations of the inflammatory cytokines (I_{12}, T_α), while the tumor volume is increasing exponentially. We can also simulate the spatial variations of the variables, but we are interested, in this paper, only in the average profiles of the variables in order to determine the tumor volume growth (or shrinkage, under treatment). We note however that the diffusion coefficients of cells and cytokines differ by several orders of magnitude, and the boundary condition (19) brings new T cells into the tumor. For these reasons an ODE system cannot adequately represent the dynamics of the tumor volume.

Bertrand et al. [32] demonstrated, in a mouse model, that TNF-α blockade overcomes resistance to anti-PD-1 in melanoma. In [32] mice were injected with 3×10^5 melanoma cells, and the tumor became detectible by day 6. Drugs (anti-PD-1 and anti-TNF-α) were injected at

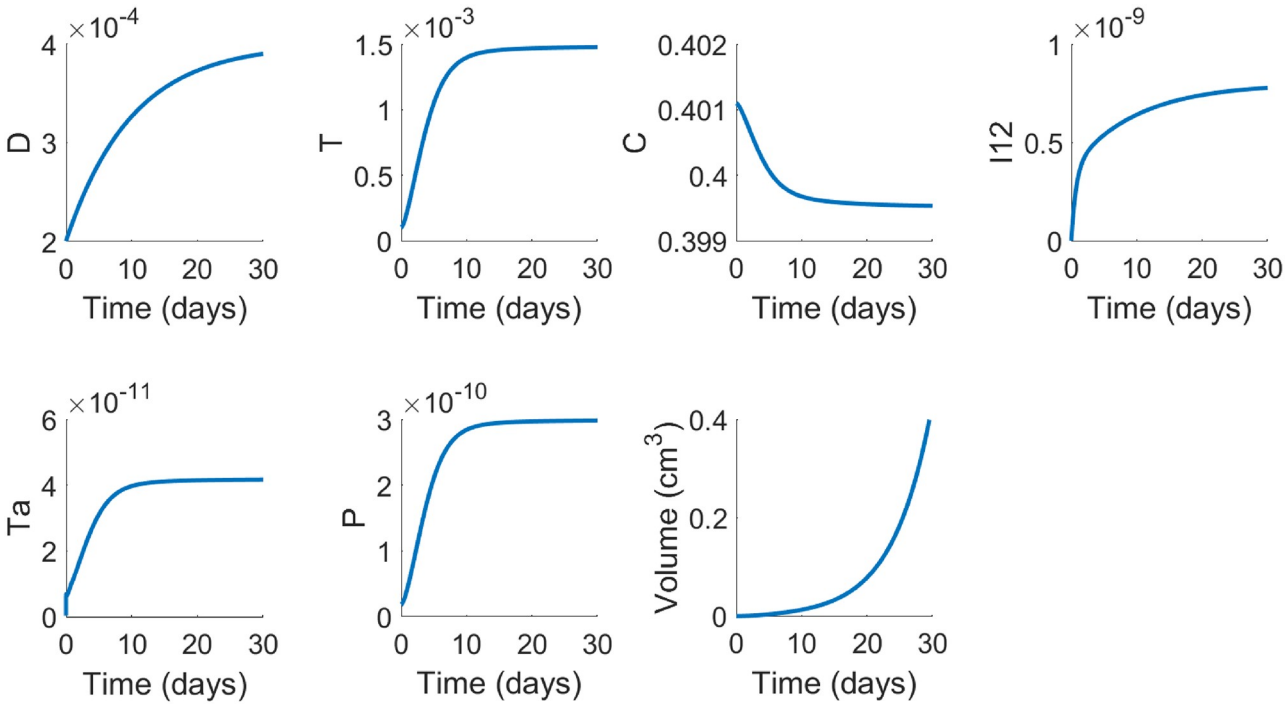

Fig 2. Average densities/concentrations, in g/cm^3, of all the variables of the model in the control case (no drugs). All parameter values are the same as in Table 2, for the mouse model.

https://doi.org/10.1371/journal.pone.0231499.g002

days 6,10,13 in (see Fig 6(d) of [32]) and at days 13, 16, 19 in (see Fig 6(e) of [32]); the tumor volume increase was in the range of 100-350 mm^3.

Fig 3 shows the growth of tumor volume under treatment with anti-PD-1 (γ_A) and anti-TNF-α (γ_B). Taking $\gamma_A = 10^{-10}$ g/cm^3 · day^{-1}, $\gamma_B = 10^{-6}$ g/cm^3 · day^{-1}, and using the same schedules of treatment as in Bertrand et al. [32], Fig 3(a) is in qualitative agreement with Figure 6(d) of Bertrand et al. [32], and Fig 3(b) is in qualitative agreement with Figure 6(e) of [32].

Clinical trials in silico

We proceed with treatment of humans, given in cycle of 3 weeks. We compare the different scheduling options in a cycle:

- (S1) Both anti-PD-1 (nivolumab) and anti-TNF-α (infliximab) are injected in the first day of week 1;
- (S2) Anti-PD-1 is injected in the first day of week 1 and anti-TNF-α is injected in the first day of week 2;
- (S3) Anti-TNF-α is injected in the first day of week 1 and anti-PD-1 is injected in the first day of week 2.

A course of cancer treatment may take 3 to 8 cycles. As in [46–48] we shall evaluate the efficacy of a treatment by the tumor volume reduction rate (TVRR) at the end-point (final day) of

Table 2. Summary of parameter values.

Notation	Description	Value used	References
δ_D	diffusion coefficient of DCs	8.64×10^{-7} cm^2 day^{-1}	[49]
δ_T	diffusion coefficient of T cells	8.64×10^{-7} cm^2 day^{-1}	[49]
δ_C	diffusion coefficient of tumor cells	8.64×10^{-7} cm^2 day^{-1}	[49]
$\delta_{I_{12}}$	diffusion coefficient of IL-12	7.17×10^{-2} cm^2 day^{-1}	estimated
δ_{T_α}	diffusion coefficient of TNF-α	8.46×10^{-2} cm^2 day^{-1}	estimated
δ_A	diffusion coefficient of anti-PD-1	4.76×10^{-2} cm^2 day^{-1}	estimated
δ_B	diffusion coefficient of anti-TNF-α	4.75×10^{-2} cm^2 day^{-1}	estimated
σ_0	flux rate of T cells at the boundary	1 cm^{-1}	[49]
η	killing rate of tumor cells by T cells	328.55 cm^3/g · day	[50]
μ_{PA}	blocking rate of PD-1 by anti-PD-1	1.03×10^7 cm^3/g · day	estimated
$\mu_{T\alpha}B$	blocking rate of TNF-α by anti-TNF-α	2.56×10^8 cm^3/g · day	estimated
ρ_P	expression of PD-1 in T cells	2.49×10^{-7}	[50]
ρ_L	expression of PD-L1 in T cells	3.25×10^{-7}	[50]
ρ_M	expression of TIM in T cells	1.5×10^{-7}	estimated
ρ_G	expression of Gal-9 in cancer cells	2×10^{-8}	estimated
ε_C	the ratio of mass of PD-L1 in cancer cell and T cell	0.1	estimated
α_L	upregulation rate of PD-L1 by TNF-α	1	estimated
α_T	upregulation rate of TIM-3 by TNF-α	1	estimated
α_{MA}	enhancement of upregulation of TIM-3 by anti-PD-1	2	estimated
$\lambda_{DC}\hat{D}_0$	activation rate of DCs by tumor cells	8×10^{-5} g/cm^3 · day	[50]
$\lambda_{TI_{12}}\hat{T}_0$	activation rate of T cells by IL-12	6.48×10^{-4} g/cm^3 · day	estimated
λ_C	growth rate of cancer cells in mice	1.295 day^{-1}	estimated
λ_C	growth rate of cancer cells in humans	0.895 day^{-1}	estimated
$\lambda_{I12}D$	production rate of IL-12 by DCs	2.76×10^{-6} day^{-1}	estimated
$\lambda_{T\alpha}T$	production rate of TNF-α by T cells	6.48×10^{-4} day^{-1}	estimated
d_D	death rate of DCs	0.1 day^{-1}	estimated
d_T	death rate of T cells	0.197 day^{-1}	estimated
d_C	death rate of tumor cells	0.17 day^{-1}	[49]
$d_{I_{12}}$	degradation rate of IL-12	1.38 day^{-1}	[51]
d_{T_α}	degradation rate of TNF-α	216 day^{-1}	[52]
d_A	degradation rate of anti-PD-1	0.046 day^{-1}	estimated
d_B	degradation rate of anti-TNF-α	0.069 day^{-1}	estimated
K_D	half-saturation of dendritic cells	4×10^{-4} g/cm^3	[50]
K_T	half-saturation of T cells	1×10^{-3} g/cm^3	[50]
K_C	half-saturation of tumor cells	0.4 g/cm^3	[49]
$K_{I_{12}}$	half-saturation of IL-12	8×10^{-10} g/cm^3	[50, 53]
K_{T_α}	half-saturation of TNF-α	3×10^{-11} g/cm^3	[54]
K_{TQ_1}	inhibition of function of T cells by PD-1-PD-L1	1.36×10^{-18} g^2/cm^6	estimated
K_{TQ_2}	inhibition of function of T cells by Tim-3-Gal-9	1.365×10^{-18} g^2/cm^6	estimated
C_M	carrying capacity of cancer cells	0.8 g/cm^3	estimated
$\hat{T}$	density of CD8$^+$ T cells from lymph node	2×10^{-3} g/cm^3	estimated
β	drug control parameter	1.55 g/cm^3	fitted

https://doi.org/10.1371/journal.pone.0231499.t002

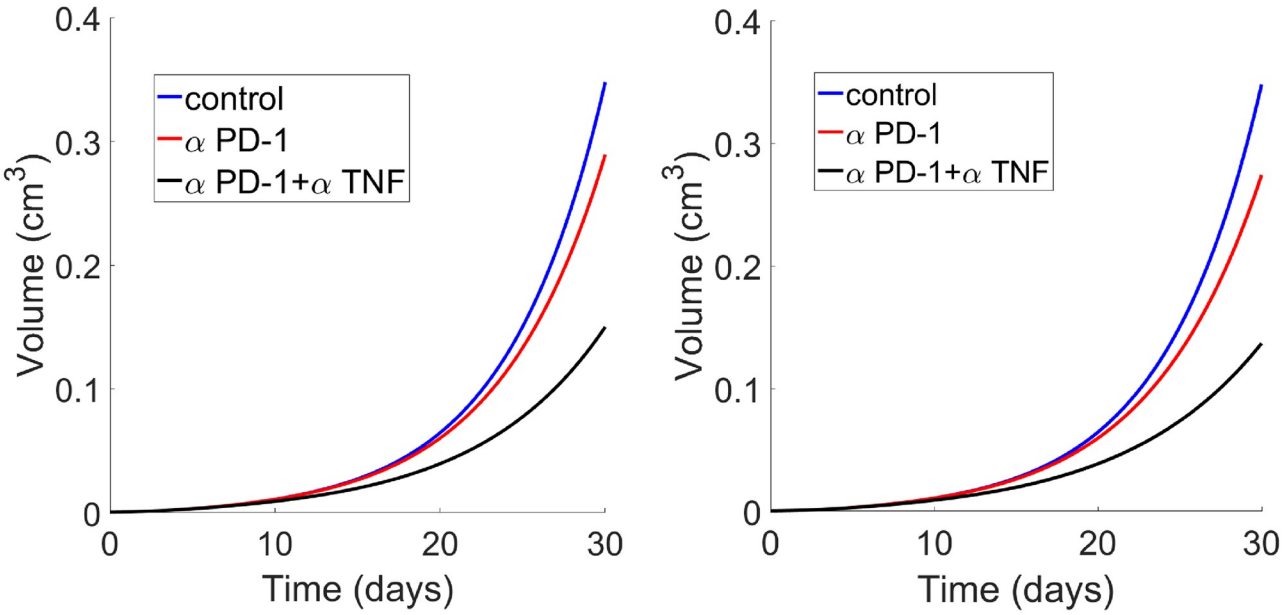

Fig 3. Growth of tumor volume without treatment, or under treatment with γ_A, or combination (γ_A, γ_B). (a) The treatment is at days 6, 10 and 13. (b) The treatment is at days 13, 16 and 19. $\gamma_A = 10^{-10}$ g/cm^3 · day, $\gamma_B = 10^{-6}$ g/cm^3 · day. All other parameter values are the same as in Table 2, for the mouse model.

https://doi.org/10.1371/journal.pone.0231499.g003

the treatment, where we define

$$\text{TVRR} = \frac{V(0) - V(t_e)}{V(0)} \times 100\%,$$

and $V(0)$ = initial tumor volume, $V(t_e)$ = end-point tumor volume.

We note that the doses γ_A and γ_B used in the model are correlated to, but not the same as, the dose amounts used in actual treatments of patients; in particular, the fact that in our model γ_B is several orders of magnitude larger than γ_A does not mean that it is relatively larger than γ_A in clinical treatment. But it is reasonable to expect that the reduction in the doses in the model will have the same effect on the tumor volume growth if the corresponding reduction was made in the treatment of patients. The doses of γ_A, γ_B in Fig 3 were chosen in order to fit the simulations with experimental results. For humans we took a smaller tumor cells growth, and smaller ranges of γ_A, γ_B in Figs 4 and 5 (below) in order to get the reduction of tumor volume to be in the same range as in clinical data; In [47], under two 3-week cycles in treatment of breast cancer, TVRR was >65%, and in [48], under four 2-week cycles treatment of rectal cancer, TVRR median was 52% but, for significant number of patients, it was >65%.

In Fig 4 we simulated the TVRR for a tumor with initial radius $R(0) = 0.5$ cm (volume 0.5236 cm^3), in the upper row, and $R(0) = 1$ cm (volume 3.1456 cm^3) in the lower row, under 5 cycle treatment course, undergoing 5 cycles with doses of γ_A and γ_B in the ranges of 0.1×10^{-11}–1×10^{-11} g/cm^3 · day and 0.1×10^{-6}–1×10^{-6} g/cm^3 · day, respectively. We see that, in the treatment of both tumors, S2 is somewhat more effective than S1, while S1 is significantly more effective than S3. We can explain this as follows:

Under S1, resistance to anti-PD-1 begins at day 1 of a cycle, but its effect may be still small in the first few days. So it is more effective to apply the resistance-blocking drug (γ_B) in the first day of week 2 of a cycle rather than immediately in day 1 of week 1. On the other hand, under schedule S3, blocking anti-PD-1 resistance when γ_A is injected in day 1 of the second

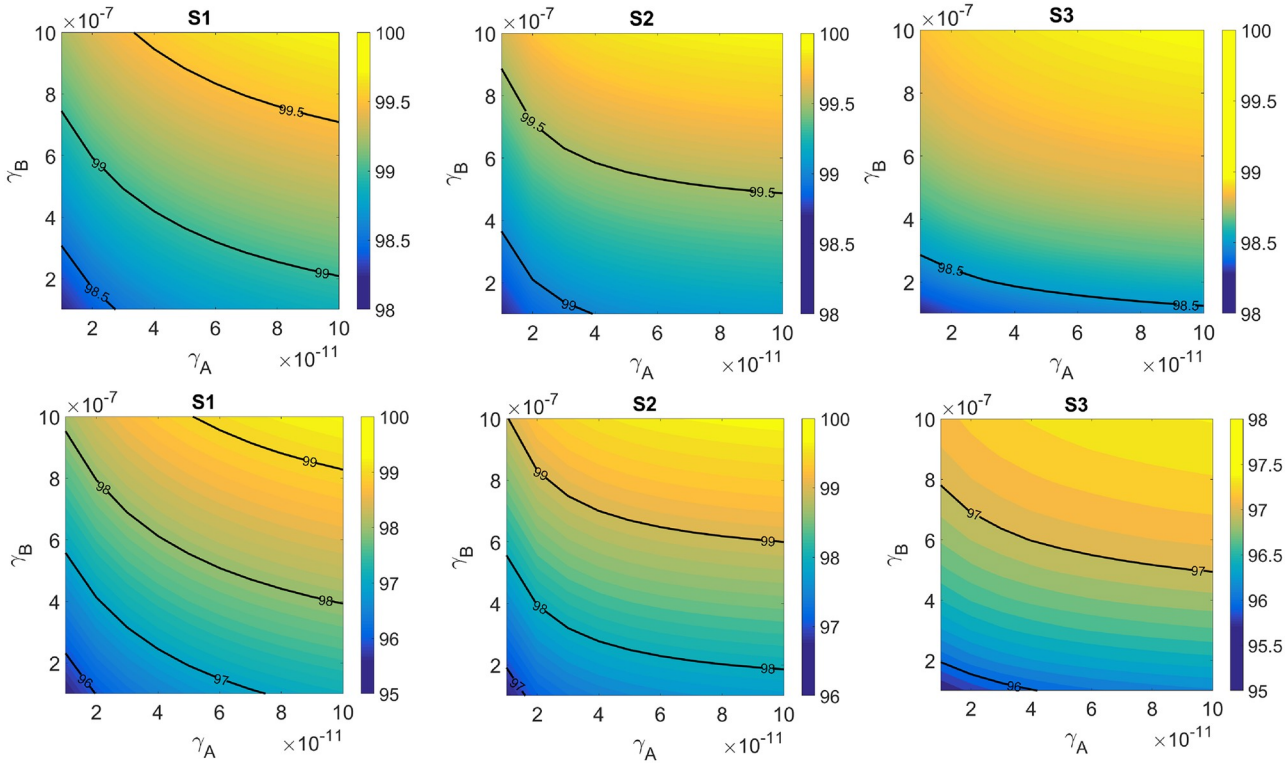

Fig 4. Efficacy map for three schedules: S1 (left), S2 (middle) and S3 (right). The color columns indicate the tumor volume reduction rate (TVRR) after 5 cycles; tumor is initially with the radius $R(0) = 0.5$ cm (upper row) and $R(0) = 1$ cm (lower row).

https://doi.org/10.1371/journal.pone.0231499.g004

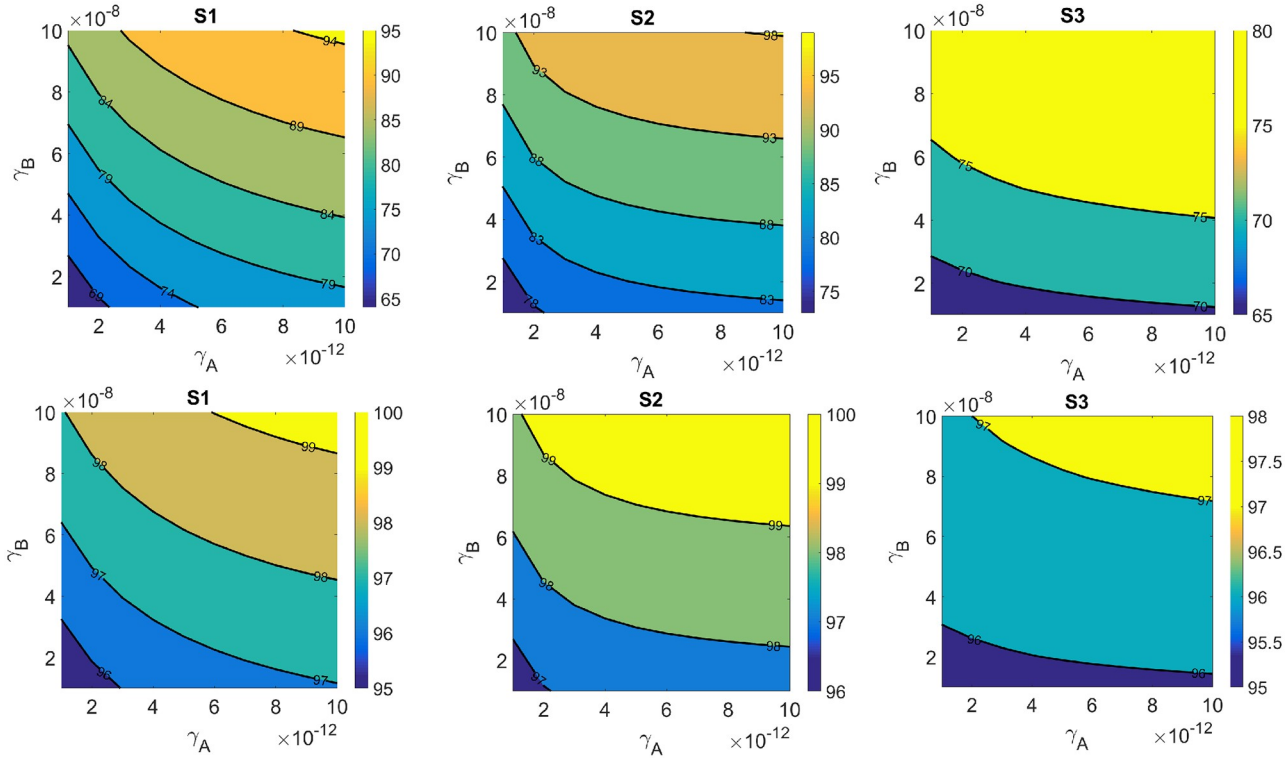

Fig 5. Efficacy map for three schedules: S1 (left), S2 (middle) and S3 (right). The color columns indicate the tumor volume reduction rate (TVRR) after 5 cycles (upper row) and 10 cycles (lower row); tumor is initially with radius $R(0) = 1$ cm.

https://doi.org/10.1371/journal.pone.0231499.g005

week of a cycle will occur only 2 weeks later when γ_B is injected in day 1 of week 1 of the following cycle. Hence the blockade of resistance comes "too late" and is not very effective. We conclude that, in order to overcome the resistance to anti-PD-1 drug (γ_A) most effectively, the anti-TNF-α drug (γ_B) should be injected not too soon but definitely not too late after the injection of γ_A.

In Fig 5 we repeated the simulations of Fig 4 with $R(0) = 1$ cm and a smaller range of doses; we did it for one treatment with 5 cycles and an extended treatment with 10 cycles. We first see that, once again, S2 is somewhat more effective than S1, and S1 is significantly more effective than S3. But we can also see from Fig 5 the benefits of extended treatment. For example, under schedule S2, with $R(0) = 1$ cm, the TVRR will increase from 75%, 85% and 90% to 96%, 97.8% and 99%, respectively, if the treatment is extended from 5 cycles to 10 cycles. By comparing the treatments with different ranges of dose, in the case of schedule S2 with $R(0) = 1$ cm, we see that if the range is decreased by a factor of 1/10 then the TVRR will decrease, for instances, from 98–99% to 82–85%. We also see from Fig 4 that under the sane treatment, the TVRR is larger for the tumor with the smaller initial volume. This can be explained by the fact that concentration of the same dose injected into a small tumor is larger than that injected into a larger tumor.

Conclusion

Drug resistance is a major obstacle to cancer treatment. Patients respond well for several months, or even years, but relapse eventually occurs. This is the case with both chemotherapy and immune therapy drugs. Anti-Cancer T cells have 'brakes' (called checkpoints) on their activities in the form of membranous proteins such as PD-1 and TIM-3; when PD-L1 (or Gal-9) combines with PD-1 (or TIM-3) the T cell activation is inhibited. A drug, anti-PD-1, is increasing used in the treatment of cancer, and in the present paper we considered the problem of how to deal with cancer resistance to anti-PD-1. We focused on the role of TNF-α in reducing this resistance.

TNF-α increases the production of PD-L1, which renders anti-PD-1 less effective. TNF-α also activates expression of TIM-3, which enables Gal-3, expressed on cancer cells, to block T cells by combing with TIM-3 on T cells membrane. These facts suggest that anti-TNF-α could be an effective drug in reducing resistance to anti-PD-1.

We developed a mathematical model where anti-PD-1 is combined with anti-TNF-α. The model is represented by a system of PDEs. The model is 'minimal' in the sense that it includes only cancer cells, T cells and dendritic cells, and the most relevant protein populations needed to address the effectiveness of the combined therapy. Simulations of the model were shown to be in agreement with mice experiments.

The model can be used to assess the efficacy of various protocols of treatment with the combination of the two drugs. As an example, we considered the following scheduling cycles.: Both drugs administered in day 1 of week 1 (S1), anti-PD-1 injected in day 1 of week 1 and anti-TNF-α injected in day 1 of week 2 (S2), or in the inverse order (S3). For each pair of (anti-PD-1, anti-TNF-α) in some range we marked on the color columns the tumor volume reduction rate (TVRR) at the end of the treatment. In Figs 4 and 5 it was shown that schedule S2 is somewhat more beneficial than schedule S1, while schedule S1 is significantly more beneficial than schedule S3; these results mean that in order for the blockade of the drug resistance to anti-PD-1, anti-TNF-α should not be injected too late after the injection of anti-PD-1, but also not too early. This result should be viewed as an hypothesis, to be validated in clinical trials.

Figs 4 and 5 also show how TVRR increases as the dose level increases when the range of doses increases by a factor of 10, or when the treatment, with the same dose range, is given to a tumor with a smaller volume.

The model developed in this paper can be used also be explore the efficacy of schedules with shorter cycles when such clinical trials become more prevalent.

Supplementary materials

Computational method

We consider the following convection-diffusion equation to illustrate our computational method:

$$\frac{\partial X}{\partial t} + div(vX) = D\nabla^2 X + F_X, \tag{25}$$

where F_X accounts for all the right-hand side terms. Since the model we consider is a free boundary problem, we employ the moving mesh method to compute it. We write Eq (25) can be written in the total derivative form

$$\frac{dX(r(t),t)}{dt} + div(v)X = D\nabla^2 X(r(t),t) + F_X.$$

Let r_i^n, X_i^n denote numerical approximations of i-th grid point and $X(r_i^n, t)$, respectively, when $t = n\tau$, where τ is the time stepsize. The discretization is derived by the explicit Euler finite difference scheme, i.e.,

$$\frac{X_i^{n+1} - X_i^n}{\tau} + \left(\frac{v_r}{r_i^n} + v_i^n\right)X_i^n = D\left(X_{rr} + \frac{X_r}{r_i^n}\right) + F_X,$$

where $X_r = \frac{h_{-1}^2 X_{i+1}^n - h_1^2 X_{i-1}^n - (h_1^2 - h_{-1}^2)X_i^n}{h_1(h_{-1}^2 - h_1 h_{-1})}$, $X_{rr} = 2\frac{h_{-1}X_{i+1}^n - h_1 X_{i-1}^n + (h_1 - h_{-1})X_i^n}{h_1(h_1 h_{-1} - h_{-1}^2)}$, and $h_{-1} = r_{i-1}^n - r_i^n$, $h_1 = r_{i+1}^n - r_i^n$. Then the mesh is moving by $r_i^{n+1} = r_i^n + v_i^n\tau$, where v_i^n is solved by the velocity equation. In order to make the Euler method stable, we take $\tau \leq \frac{min\{h_1, h_{-1}\}}{2D}$.

Parameter estimation

Half-saturation. In an expression $Y\frac{X}{K_X + X}$ which represents an activation of a species Y by a species X, the parameter K_X is called the "half-saturation" of X. We assume that the average density/concentration of each species, X, tends to steady state X^0, and that the quotient $X^0/(K_X + X^0)$ is not too close to 0 or to 1, and take

$$\frac{X^0}{K_X + X^0} = \frac{1}{2}, \text{ or } K_X = X^0. \tag{26}$$

The values X^0 will be estimated from clinical/experimental data, and then the K_X are determined by (26).

Diffusion coefficients. Young [55] established the following formula for the diffusion coefficient, D_p, of any protein p:

$$D_p = \frac{A}{M_p^{1/3}}, \tag{27}$$

where M_p is the molecular weight of p and A is a constant. In particular

$$D_p = \frac{M_V^{1/3}}{M_p^{1/3}} D_V, \tag{28}$$

where M_V and D_V are respectively the molecular weight and diffusion coefficient of VEGF: M_V = 24kDa [56] and $D_V = 8.64 \times 10^{-2}$ cm^{-2}d^{-1} [57]. The following table lists the molecular weight of the proteins in our model, taken from [56], and their corresponding diffusion coeffi-

X	I_{12}	T_α
Molecular Weight(kDa)	37.2	25.6
D_X (10^{-2} cm^{2}d^{-1})	7.17	8.46

cients computed from the formula (28): The molecular weights of nivalumab (A) and infliximab (B) are 143.6 kDa and 144.2 kDa, respectively. Hence, by formula (28), we get $D_A = 4.76 \times 10^{-2}$ cm^{2}d^{-1} and $D_B = 4.75 \times 10^{-2}$ cm^{2}d^{-1}.

Diffusion coefficients of cells. For simplicity, we assume that all cell types have the same diffusion coefficient, and as in [57], we take

$$D_X = 8.64 \times 10^{-7} \text{ cm}^2\text{d}^{-1},$$

Death/Degradation rates. From [58] we take d_T = 0.18/d, and from [49] we take d_D = 0.1/d and d_C = 0.17/d. The half-life of I_{12} in peripheral blood is 352 minutes and in chord blood 614 minutes [51]. We accordingly take the half-life of I_{12} in tissue to be 5 hours, so that $d_{I_{12}} = 1.38/\text{d}$. The half-life of TNF-$\alpha$ is 4.6 minutes [52]; hence, $d_{T_\alpha} = 216/\text{d}$.

Inhibition of T by Q_1, Q_2. From the notation $K'_{TQ_1} = \sigma_1 K_{TQ}$, we deduce, as in [59], that $K_{TQ_1} = 1.36 \times 10^{-18}\text{g/cm}^3$. We assume a similar inhibition parameter for the checkpoint T_M, taking $K_{TQ_2} = 1.365 \times 10^{-18}\text{g/cm}^3$.

Production parameters. In order to estimate production parameters, we use the "steady-state" of each equation, that is, we equate the right-hand side of each equation to zero, replace each species X in this equation by X^0 and each K_X by X^0.

Eq (2). In steady state, we have

$$\lambda_{DC} \frac{\hat{D}_0}{2} = d_D D^0,$$

The number of dendritic cells in advanced melanoma can increase to 400 cells/mm^3 [60]. Taking it to be 200 cells/mm^3 and assuming that the mass of one DC is 5×10^{-10} g, we get $D^0 = 4 \times 10^{-4}$. Since d_D = 0.1/day [49], we obtain

$$\lambda_{DC} \hat{D}_0 = 2 d_D K_D = 8 \times 10^{-5}.$$

Eq (3). we assume that in steady state,

$$\frac{1}{1 + PL/K_{TQ_1}} \frac{1}{1 + T_M G/K_{TQ_2}} = \frac{1}{1.8}$$

Hence, in steady state of Eq (3),

$$\lambda_{TI_{12}}\hat{T}_0 \cdot \frac{1}{2} \cdot \frac{1}{1.8} - d_T T^0 = 0.$$

The number of $CD8^+$ T cells in melanoma is in the range of $7 - 10 \times 10^5$ cells/cm^3 [61]. Taking the mass of one cells to be 5×10^{-10}, we estimate the density of $CD8^+$ T cells at 5×10^{-4} g/cm^3. Since T includes Th1 cells, we take $K_T = T^0 = 10^{-3}$ g/cm^3. Since $d_T = 0.18$/day [58], we get $\lambda_{TI_{12}}\hat{T}_0 = 6.48 \times 10^{-4}$ g/cm^3/day.

Eq (4). We take, in steady state, $C = 0.4$ g/cm^3 [49] and $C_M = 0.8$ g/cm^3, $\eta = 328$ 0.8 g/cm^3/g $\cdot$ day^{-1} [50], $d_C = 0.17$/day [58]. Hence, in steady state,

$$\lambda_C \cdot \frac{1}{2} - \eta K_T - d_C = 0,$$

so that $\lambda_C = 0.996$/day. Since, however, the tumor volume is increasing on account of the abnormal proliferation of cancer cells, we increase this value by a factor, taking $\lambda_C = 1.2 \times 0.996 = 1.295$/day. This value will be used in mouse models, as in Figs 2 and 3. But for humans (Figs 4 and 5) it is assumed that the tumor cells proliferation is slower, taking $\lambda_C = 0.885$/day.

Eq (5). From the steady state equation we get

$$\lambda_{I_{12}D}K_D - d_{I_{12}}K_{I_{12}} = 0.$$

Since $K_D = 4 \times 10^{-4}$ g/cm^3, $K_{I_{12}} = 8 \times 10^{-10}$g/cm^3 [50, 53], and $d_{I_{12}} = 1.38/\text{day}$ [51], we get $\lambda_{I12}\, D = 2.76 \times 10^{-6}$/day.

Eq (6). From the steady state equation in the control case we get

$$A_{T_\alpha} + \lambda_{T_\alpha T}K_T - d_{T_\alpha}K_{T_\alpha} = 0.$$

We take $A_{T_\alpha} = 1.12 \times 10^{-9}$ g/cm^3day. Since $K_{T_\alpha} = 3 \times 10^{-11}$g/cm^3 [54] and $d_{T_\alpha} = 216/\text{day}$ [52], we get $\lambda_{T\alpha}\, T = 1.08 \times 10^{-6}$/day.

Remaining parameters. We take $\rho_P = 2.49 \times 10^{-7}$ [50]. Then, in steady state with $T = K_T = 10^{-3}$ g/cm^3 and $P = 2.49 \times 10^{-10}$ g/cm^3. We take $\rho_L = 3.25 \times 10^{-7}$ g/cm^3 [50] and assume that the expression of PD-L1 in cancer cells is less than it is on T cells, taking $\varepsilon_C = 0.1$ in Eq (8). We also take $\alpha_L = 1$ which means that TNF-α increases the expression of PD-L1 by 50%, in steady state.

We assume that TIM-3 is expressed on T cells at a lower level than PD-1, that is, $\rho_M < \rho_P$, and take

$$\rho_M = 1.5 \times 10^{-7}.$$

We also take (in Eq (11)) $\alpha_T = 1$ and $\alpha_{MA} = 2$. We similarly assume that Gal-9 is expressed in cancer cells at a lower level than PD-L1 (in Eq (8)), that is, $\rho_G < \rho_L\, \varepsilon_C$, and take $\rho_G = 2 \times 10^{-8}$.

The half-life od nivolumab is 10-20 days. Taking it to be 15 days, we get

$$d_A = \frac{\ln 2}{15} = 0.046 \text{ day}^{-1}.$$

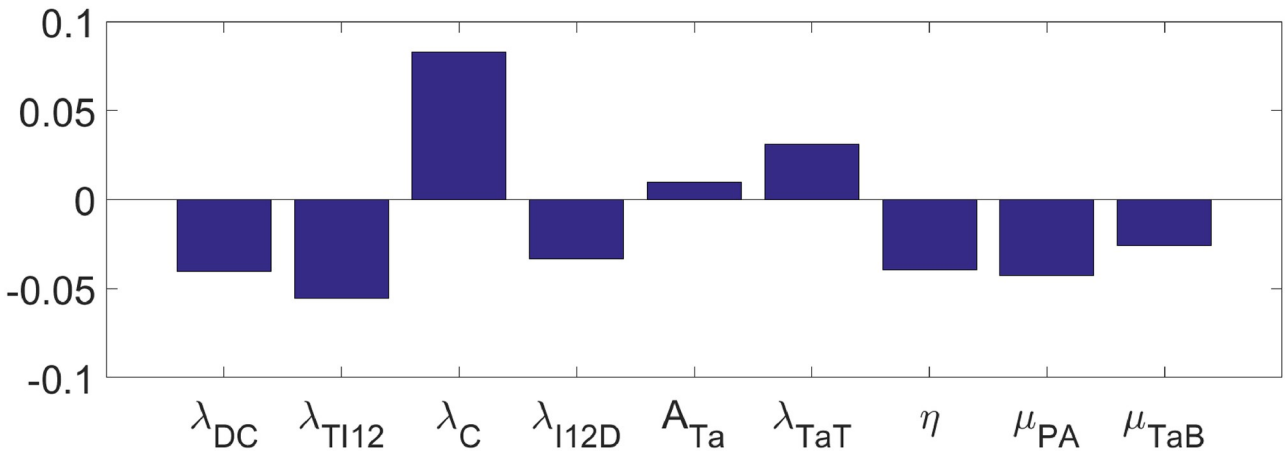

Fig 6. Sensitivity analysis of the PRCC values with respect to the radius of the tumor.

https://doi.org/10.1371/journal.pone.0231499.g006

The half-life of infliximab is 7-12 days. Taking half-life of 10 days, we get

$$d_B = \frac{\ln 2}{10} = 0.069 \text{ day}^{-1}.$$

We assume that 10% of A is used in blocking PD-L1 while the remaining 90% degrades naturally or decreased by washout, that is

$$\mu_{PA} PA/10\% = d_A A/90\%.$$

Recalling that, in steady state, with $P = 2.49 \times 10^{-10}$, g/cm^3, we get

$$\mu_{PA} = \frac{0.046}{9 \times 2.49 \times 10^{-10}} = 1.03 \times 10^7 \text{ cm}^3/\text{g} \cdot \text{day}.$$

Under a similar assumption on the depletion of B, in steady state

$$\mu_{T_\alpha B} = \frac{d_B}{9K_{T_\alpha}} = \frac{0.069}{9 \times 3 \times 10^{-11}} = 2.56 \times 10^8 \text{ cm}^3/\text{g} \cdot \text{day}.$$

Sensitivity analysis

We performed sensitivity analysis on the production parameters in Eqs (2)–(6), the depletion rates μ_{BT_α} and μ_{PA} in Eqs (6) and (9), and η in Eq (4). Following the method in [62], we performed Latin hypercube sampling and generated 1000 samples to calculate the partial rank correlation (PRCC) and the p-values with respect to the radius of the tumor at day 30. The results are shown in Fig 6 (The p-value was <0.01). Note that as T_α increases, cancer increases. Hence A_{T_α}, $\lambda_{T\alpha}$ T are positively correlated and $\mu_{T\alpha}$ B is negatively correlated. On the other hand, as T increases, cancer decreases. Hence λ_{DC}, $\lambda_{TI_{12}}$, λ_{I12} D and μ_{PA} (in Fig 6) are negatively correlated. Finally the killing rate η of C by T is negatively correlated while the growth rate λ_C of C is highly positively correlated.

Acknowledgments

The authors thank Mathematical Biosciences Institute for the support of this collaboration. WH was partially supported by the National Science Foundation (Grant DMS-1818769). XL

was partially supported by the Fundamental Research Funds for the Central Universities (19XNLG14), and the Research Funds of Renmin University of China, and the National Natural Science Foundation of China (No.11571364).

Author Contributions

Conceptualization: Xiulan Lai, Wenrui Hao, Avner Friedman.

Formal analysis: Xiulan Lai, Wenrui Hao, Avner Friedman.

Funding acquisition: Xiulan Lai, Wenrui Hao.

Investigation: Xiulan Lai, Wenrui Hao, Avner Friedman.

Project administration: Xiulan Lai, Wenrui Hao, Avner Friedman.

Supervision: Avner Friedman.

Validation: Xiulan Lai, Wenrui Hao, Avner Friedman.

Writing – original draft: Xiulan Lai, Wenrui Hao, Avner Friedman.

Writing – review & editing: Xiulan Lai, Wenrui Hao, Avner Friedman.

References

1. Leonard GD, Fojo T, Bates SE. The role of ABC transporters in clinical practice. Oncologist. 2003; 8(5):411–424. https://doi.org/10.1634/theoncologist.8-5-411 PMID: 14530494
2. Cree IA, Charlton P. Molecular chess? Hallmarks of anti-cancer drug resistance. BMC Cancer. 2017 Jan; 17(10):1–8.
3. Khunweeraphong N, Stockner T, Kuchler K. The structure of the human ABC transporter ABCG2 reveals a novel mechanism for drug extrusion. Scientific Reports. 2017 Oct; 7(13767):1–15.
4. Gillet JP, Gottesman MM. Mechanisms of Multidrug Resistance in Cancer. Methods in molecular biology multi-drug resistance in cancer. 2009; 596:47–76. https://doi.org/10.1007/978-1-60761-416-6_4
5. Komarova NL, Wodarz D. Drug resistance in cancer: Principles of emergence and prevention. Proceedings of the National Academy of Sciences. 2005; 102(27):9714–9719. https://doi.org/10.1073/pnas.0501870102
6. Tomasetti C, Levy D. Role of symmetric and asymmetric division of stem cells in developing drug resistance. ProcNatl Acad Sci USA. 2010; 107(39):16766–16771. https://doi.org/10.1073/pnas.1007726107
7. Lavi O, Gottesman MM, Levy D. The dynamics of drug resistance: A mathematical perspective. Drug Resistance Updates. 2012; 15(1-2):90–97. https://doi.org/10.1016/j.drup.2012.01.003 PMID: 22387162
8. Wooten DJ, Quaranta V. Mathematical models of cell phenotype regulation and reprogramming: Make cancer cells sensitive again! Biochimica et Biophysica Acta (BBA)—Reviews on Cancer. 2017; 1867 (2):167–175. Available from: https://doi.org/10.1016/j.bbcan.2017.04.001.
9. Rockne RC, Hawkins-Daarud A, Swanson KR, Sluka J, Glazier JA, Macklin P, et al. The 2019 mathematical oncology roadmap. Phys Biol. 2019; 16(4):041005. https://doi.org/10.1088/1478-3975/ab1a09 PMID: 30991381
10. Feizabadi MS. Modeling multi-mutation and drug resistance: analysis of some case studies. Theoretical Biology and Medical Modelling. 2017; 14(1). https://doi.org/10.1186/s12976-017-0052-y PMID: 28327183
11. Hadjiandreou MM, Mitsis GD. Mathematical Modeling of Tumor Growth, Drug-Resistance, Toxicity, and Optimal Therapy Design. IEEE Transactions on Biomedical Engineering. 2014; 61(2):415–425. https://doi.org/10.1109/TBME.2013.2280189 PMID: 24021634
12. Sun X, Hu B. Mathematical modeling and computational prediction of cancer drug resistance. Briefings in Bioinformatics. 2018; 19(6):1382–1399. Available from: http://dx.doi.org/10.1093/bib/bbx065. PMID: 28981626
13. Zanudo JGT, Steinway SN, Albert R. Discrete dynamic network modeling of oncogenic signaling: Mechanistic insights for personalized treatment of cancer. Current Opinion in Systems Biology. 2018; 9:1–10. Available from: https://doi.org/10.1016/j.coisb.2018.02.002.

14. Gaffney Ea. The application of mathematical modelling to aspects of adjuvant chemotherapy scheduling. Journal of Mathematical Biology. 2004; 48(4):375–422. https://doi.org/10.1007/s00285-003-0246-2 PMID: 15052504

15. Cho H, Levy D. Modeling continuous levels of resistance to multidrug therapy in cancer. Applied Mathematical Modelling. 2018; 64:733–751. https://doi.org/10.1016/j.apm.2018.07.025

16. Cho H, Levy D. Modeling the chemotherapy-induced selection of drug-resistant traits during tumor growth. Journal of Theoretical Biology. 2018; 436:120–134. https://doi.org/10.1016/j.jtbi.2017.10.005 PMID: 29030212

17. Zaretsky MJ, GarciaDiaz A, Shin DS, Escuin-Ordinas H, Hugo W, Hu-Lieskovan S, et al. Mutations Associated with Acquired Resistance to PD-1 Blockade in Melanoma. N Engl J Med. 2016 Sep; 375 (9):819–829. https://doi.org/10.1056/NEJMoa1604958 PMID: 27433843

18. Sucker A, Zhao F, Real B, Heeke C, Bielefeld N, Maben S, et al. Genetic evolution of T-cell resistance in the course of melanoma progression. Clin Cancer Res. 2014 Dec; 20(24):6593–6604. https://doi.org/10.1158/1078-0432.CCR-14-0567 PMID: 25294904

19. Sade-Feldman M, Jiao YJ, Chen JH, Rooney MS, Barzily-Rokni M, Eliane JP, et al. Resistance to checkpoint blockade therapy through inactivation of antigen presentation. Nature Communicationsvolume. 2017 Oct; 8(1136):1–15.

20. Jenkins RW, Barbie DA, Flaherty KT. Mechanisms of resistance to immune checkpoint inhibitors. British Journal of Cancer. 2018 Jan; 118(1):9–16. https://doi.org/10.1038/bjc.2017.434 PMID: 29319049

21. Shin DS, Zaretsky M Jesse, Escuin-Ordinas H, Garcia-Diaz A, Hu-Lieskovan S, Kalbasi A, et al. Primary Resistance to PD-1 Blockade Mediated by JAK1/2 Mutations. Cancer Discov. 2017 Feb; 7 (2):188–201. https://doi.org/10.1158/2159-8290.CD-16-1223 PMID: 27903500

22. Garcia-Diaz A, Shin DS, Moreno BH, Saco J, Escuin-Ordinas H, Rodrigue GA, et al. Interferon Receptor Signaling Pathways Regulating PD-L1 and PD-L2 Expression. Cell Rep. 2017 May; 19(6):1189–1201. https://doi.org/10.1016/j.celrep.2017.04.031 PMID: 28494868

23. Anagnostou V, Smith KN, Forde PM, Niknafs N, Bhattacharya R, White J, et al. Evolution of Neoantigen Landscape during Immune Checkpoint Blockade in Non-Small Cell Lung Cancer. Cancer Discov. 2017 Mar; 7(31):264–276. https://doi.org/10.1158/2159-8290.CD-16-0828 PMID: 28031159

24. Shayan G, Srivastav R, Li J, Schmitt N, Kane LP, Ferris RL. Adaptive resistance to anti-PD1 therapy by Tim-3 upregulation is mediated by the PI3K-Akt pathway in head and neck cancer. Oncoimmunology. 2017 Dec; 6(1):e1261779. https://doi.org/10.1080/2162402X.2016.1261779 PMID: 28197389

25. Zhu C, Anderson AC, Schubart A, Xiong H, Imitola J, Khoury SJ, et al. The Tim-3 ligand galectin-9 negatively regulates T helper type 1 immunity. Nature Immunology. 2005; 6(12):1245–1252. https://doi.org/10.1038/ni1271 PMID: 16286920

26. Chou FC, Chen HY, Kuo CC, Sytwu HK. Role of Galectins in Tumors and in Clinical Immunotherapy. International Journal of Molecular Sciences. 2018 Jan; 19(2):430. https://doi.org/10.3390/ijms19020430

27. Sharma P, Hu-Lieskovan S, Wargo JA, Ribas A. Primary, Adaptive, and Acquired Resistance to Cancer Immunotherapy. Cell. 2017 Feb; 168(4):707–723. https://doi.org/10.1016/j.cell.2017.01.017 PMID: 28187290

28. Larkin J, Chiarion-Sileni V, Gonzalez R, Grob JJ, Cowey CL, Lao CD, et al. Combined Nivolumab and Ipilimumab or Monotherapy in Untreated Melanoma. N Engl J Med. 2015 Jul; 373(1):23–34. https://doi.org/10.1056/NEJMoa1504030 PMID: 26027431

29. Postow MA, Chesney J, Pavlick AC, Robert C, Grossmann K, McDermott D, et al. Nivolumab and ipilimumab versus ipilimumab in untreated melanoma. N Engl J Med. 2015 May; 372(21):2006–2017. https://doi.org/10.1056/NEJMoa1414428 PMID: 25891304

30. Wolchok JD, Kluger H, Callahan MK, Postow MA, Rizvi NA, Lesokhin AM, et al. Nivolumab plus ipilimumab in advanced melanoma. N Engl J Med. 2013 Jul; 369(2):122–133. https://doi.org/10.1056/NEJMoa1302369 PMID: 23724867

31. Seidel JA, Otsuka A, Kabashima K. Anti-PD-1 and Anti-CTLA-4 Therapies in Cancer: Mechanisms of Action, Efficacy, and Limitations. Front Oncol. 2018 Mar; 8(86):122–133.

32. Bertrand F, Montfort A, Marcheteau E, Imbert C, Gilhodes J, Filleron T, et al. TNF-alpha blockade overcomes resistance to anti-PD-1 in experimental melanoma. Nat Commun. 2017 Dec; 8(2256):1–13.

33. Lim SO, Li CW, Xia W, Cha JH, Chan LC, Wu Y, et al. Deubiquitination and Stabilization of PD-L1 by CSN5. Cancer Cell. 2016 Dec; 30(6):925–939. https://doi.org/10.1016/j.ccell.2016.10.010 PMID: 27866850

34. Donia M, Andersen R, Kjeldsen JW, Fagone P, Munir S, Nicoletti F, et al. Aberrant Expression of MHC Class II in Melanoma Attracts Inflammatory Tumor-Specific CD4 T- Cells, Which Dampen CD8 T-cell

Antitumor Reactivity. Cancer Research. 2015; 75(18):3747–3759. https://doi.org/10.1158/0008-5472.CAN-14-2956 PMID: 26183926

35. Sims GP, Rowe DC, Rietdijk ST, Herbst R, Coyle AJ. HMGB1 and RAGE in inflammation and cancer. Annu Rev Immunol. 2010; 28:367–388. https://doi.org/10.1146/annurev.immunol.021908.132603 PMID: 20192808

36. Palucka J, Banchereau J. Cancer immunotherapy via dendritic cells. Nat Rev Cancer. Mar 2012; 12 (4):265–277. https://doi.org/10.1038/nrc3258 PMID: 22437871

37. Saenz R, Futalan D, Leutenez L, Eekhout F, Fecteau JF, Sundelius S, et al. TLR4-dependent activation of dendritic cells by an HMGB1-derived peptide adjuvant. J Transl Med. Aug 2014; 12(211):1–11.

38. Janco JMT, Lamichhane P, Karyampudi L, Knutson KL. Tumor-infiltrating dendritic cells in cancer pathogenesis. J Immunol. Apr 2015; 194(7):2985–2991. https://doi.org/10.4049/jimmunol.1403134

39. Ma Y, Shurin GV, Peiyuan Z, Shurin MR. Dendritic Cells in the Cancer Microenvironment. J Cancer. 2013; 4(1):36–44. https://doi.org/10.7150/jca.5046 PMID: 23386903

40. Chen Y, Zhang X. Pivotal regulators of tissue homeostasis and cancer: macrophages. Experimental Hematology & Oncology. 2017 Aug; 6(1).

41. Cheng X, Veverka V, Radhakrishnan A, Waters LC, Muskett FW, Morgan SH, et al. Human PD-L1/B7-H1/CD274 Protein. Sino Biological Inc, http://wwwsinobiologicalcom/PD-L1-B7-H1-CD274-Protein-g-533html;.

42. Shi L, Chen S, Yang L, Li Y. The role of PD-1 and PD-L1 in T-cell immune suppression in patients with hematological malignancies. J Hematol Oncol. Sep 2013; 6(74).

43. Muppidi MR, George S. Immune Checkpoint Inhibitors in Renal Cell Carcinoma. Journal of Targeted Therapies in Cancer 2015. 2015; 4:47–52.

44. Mautea RL, Gordona SR, Mayere AT, McCrackena MN, Natarajane A, Ring NG, et al. Engineering high-affinity PD-1 variants for optimized immunotherapy and immuno-PET imaging. Proc Natl Acad Sci USA. Nov 2015; 112(47):E6506–14. https://doi.org/10.1073/pnas.1519623112

45. D'Acunto B. Computational Methods for PDE in mechanics. Series on Advances in Mathematics for Applied Sciences-Vol.67. Singapore: Word Scientific; 2004.

46. He X, Zhang Y, Ma Y, Zhou T, Zhang J, Hong S, et al. Optimal tumor shrinkage predicts long-term outcome in advanced nonsmall cell lung cancer (NSCLC) treated with target therapy. Medicine. 2016; 95 (31). https://doi.org/10.1097/MD.0000000000004176

47. Martincich L, Montemurro F, Rosa GD, Marra V, Ponzone R, Cirillo S, et al. Monitoring Response to Primary Chemotherapy in Breast Cancer using Dynamic Contrast-enhanced Magnetic Resonance Imaging. Breast Cancer Research and Treatment. 2004; 83(1):67–76. https://doi.org/10.1023/B:BREA.0000010700.11092.f4 PMID: 14997056

48. Xiao J, Cai Z, Li W, Yang Z, Gong J, Huang Y, et al. Tumor Volume Reduction Rate Predicts Pathologic Tumor Response of Locally Advanced Rectal Cancer Treated with Neoadjuvant Chemotherapy alone: Results from a Prospective Trial. Journal of Cancer. 2015; 6(7):636–642. https://doi.org/10.7150/jca.11738 PMID: 26078794

49. Friedman A, Hao W. The Role of Exosomes in Pancreatic Cancer Microenvironment. Bull Math Biol. 2017 May; 80(5):1111–1133. https://doi.org/10.1007/s11538-017-0254-9 PMID: 28382422

50. Lai X, Stiff A, Duggan M, Wesolowski R, Carson WE, Friedman A. Modeling combination therapy for breast cancer with BET and immune checkpoint inhibitors. Proc Natl Acad Sci. 2018; 115(21):5534–5539. https://doi.org/10.1073/pnas.1721559115 PMID: 29735668

51. Lee SM, Suen Y, Qian J, Knoppel E, Cairo MS. The Regulation and Biological Activity of Interleukin 12. Leukemia & Lymphoma. 1998; 29(5-6):427–438. https://doi.org/10.3109/10428199809050903

52. Simo R, Barbosa-Desongles A, Lecube A, Hernandez C, Selva DM. Potential Role of Tumor Necrosis Factor-α in Downregulating Sex Hormone-Binding Globulin. Diabetes. 2011; 61(2):372–382. https://doi.org/10.2337/db11-0727 PMID: 22210320

53. Chen LH, Song JL, Qian Y, Zhao X, Suo HY, Li J. Increased preventive effect on colon carcinogenesis by use of resistant starch (RS3) as the carrier for polysaccharide of Larimichthys crocea swimming bladder. Int J Mol Sci. 2014 Jan; 15(1):817–829. https://doi.org/10.3390/ijms15010817 PMID: 24413751

54. Hao W, Komar HM, Hart PA, Conwell DL, Lesinski GB, Friedman A. A mathematical model of chronic pancreatitis. Proc Natl Acad Sci USA. 2017 May; 114(19):5011–5016. https://doi.org/10.1073/pnas.1620264114 PMID: 28439020

55. Young ME, Carroad PA, Bell RL. Estimation of diffusion coefficients of proteins. Biotechnology and Bioengineering. 1980; 22(5):947–955. https://doi.org/10.1002/bit.260220504

56. PhosphoSitePlus, 2014: mutations, PTMs and recalibrations. Nucleic Acids Reserch—PhosphoSitePlus(R) (PSP, http://www.phosphosite.org/);43.

57. Liao KL, Bai XF, Friedman A. Mathematical Modeling of Interleukin-27 Induction of Anti-Tumor T Cells Response. PLoS ONE. 2014; 9(3):e91844. https://doi.org/10.1371/journal.pone.0091844 PMID: 24633175

58. Friedman A, Lai X. Combination therapy for cancer with oncolytic virus and checkpoint inhibitor: A mathematical model. Plos One. 2018 Aug; 13(2):e0192449. https://doi.org/10.1371/journal.pone.0192449 PMID: 29420595

59. Lai X, Friedman A. Combination therapy of cancer with cancer vaccine and immune checkpoint inhibitor: A mathematical model. PLoS ONE. 2017; 12(5):e0178479. https://doi.org/10.1371/journal.pone.0178479 PMID: 28542574

60. Vescovi R, Monti M, Moratto D, Paolini L, Consoli F, Benerini L, et al. Collapse of the Plasmacytoid Dendritic Cell Compartment in Advanced Cutaneous Melanomas by Components of the Tumor Cell Secretome. Cancer Immunol Res. 2019 Jan; 7(1):12–28. https://doi.org/10.1158/2326-6066.CIR-18-0141 PMID: 30401679

61. Lisiero DN, Soto H, Liau LM, Prins RM. Enhanced sensitivity to IL-2 signaling regulates the clinical responsiveness of IL-12-primed CD8(+) T cells in a melanoma model. J Immunol. 2011 May; 186 (9):5068–5077. https://doi.org/10.4049/jimmunol.1003317 PMID: 21430221

62. Marino S, Hogue I, Ray C, Kirschner D. A methodology for performing global uncertainty and sensitivity analysis in systems biology. J Theor Biol. 2008; 254(1):178–196. https://doi.org/10.1016/j.jtbi.2008.04.011 PMID: 18572196